Chapter 3 Relaxation Dynamics of PPB nanoparticles

3.1 Introduction

Organic nanoparticles have attracted tremendous research interests over the past few years, owing to their special properties which lie between the properties of free molecules and those of bulk materials.[1] The electronic properties in organic nanoparticles are different from those of the inorganic ones[2] because of the weak intermolecular interaction forces of the van der waals type or the hydrogen bond.[3] However, organic nanocrystals are expected to be useful as novel functional materials in electronics and photonics, because of their variability and flexibility in synthesizing materials, preparing nanoparticles, and investigating their physicochemical properties such as luminescence[4] or high nonlinear optical efficiency.[5] In the other words, the size-dependent absorption and emission is also an interesting topic for the fundamental research.[6] Nakanishi and co-workers first initiated the investigation on this topic, they focused on nanocrystal fabrications and characterizations for perylene[6a-c] and many other organic systems.[6e,f] Recent investigations on the

[1] Horn, D.; Rieger, J. *Angew. Chem. Int. Ed.* **2001**, *40*, 4330.
[2] (a)Forrest, S. *MRS Bull.* **2001**, *26*, 108. (b)Alivistos., A. P. *Science* **1996**, *271*, 933.(c)Peng, X. G. *J. Am. Chem. Soc.* **1997**, *119*, 7019.
[3] Silinsh, E. A. *Organic Molecular Crystals: Their Electronic States*; Springer-Verlag: Berlin, 1980
[4] Yoshikava, H.; Masuhara, H. *J. Photochem. Photobiol. C* **2000**, 1, 57.
[5] (a)Chemla, D. S.; Zyss, J. *Nonlinear Optical Properties of Organic Molecules and Crystals*; Academic Press: Orlando, 1987; vol 1 (b)Gehr, R. J.; Boyd, R. W. *Chem. Mater.* **1996**, *8*, 1807.
[6] (a)Kasai, H.; Kamatani, H.; Okada, S.; Oikawa, H.; Matsuda, H.; Nakanishi, H. *Jpn. J. Appl. Phys.* **1996**, *35*, L221.(b)Onodera, T.; Kasai, H., Okada, S.;Oikawa, H.; Mizuno, K.; Fujitsuka, M.; Ito, O.; Nakanishi, H. *Optical Materials* **2002**, *21*, 595. (c)Oikawa, H.; Mitsui, T.; Onodera, T.; Kasai, H.; Nakanishi, H.; Sekiguchi, T. *Jpn. J. Appl. Phys.* **2003**, *42*, L111. (d)Katagi, H.; Kasai, H.; Okada, S.; Oikawa, H.; Komatsu, K.; Matsuda, H.; Liu, Z.; Nakanishi, H. *Jpn. J. Appl. Phys.* **1996**, *35*, L1364. (e) Baba, K.; Kasai, H.; Okada, S.; Oikawa, H.; Nakanishi, H. *Optical Materials* **2002**, *21*, 591. (f) Takahashi, H.; Miura, H.; Kasai, H.; Okada, S.; Oikawa, H.; Nakanishi, H. *J. Am. Chem. Soc.* **2002**, *124*, 10944.

nanoparticles of the pyrazoline derivatives[7] indicate that the emission color is affected by the particle sizes or the excitation wavelengths. Moreover, enhanced emissions due to aggregation have been reported for the organic systems of 1-cyano-trans-1,2-bis-(4¢-methylbiphenyl)ethylene (CN-MBE).[8]

In the present study, we collaborate with Prof. Chain-Shu Hsu for the synthesizing of 1,4-di[(E)-2-phenyl-1-propenyl]benzene (PPB, the structure is shown in scheme 1). This compound belongs to the family of phenylenevinylenes (PV) with two methyl groups added to 1,4-distyrylbenzene (DSB) skeleton. It is observed that the fluorescent emission from PPB nanoparticles is extremely strong, but PPB itself is non-fluorescent in dilute solution, which is similar to the feature observed in CN-MBE.[8] In contrast, free DSB in solution is highly fluorescent, but its nanoparticle shows low-emission feature.

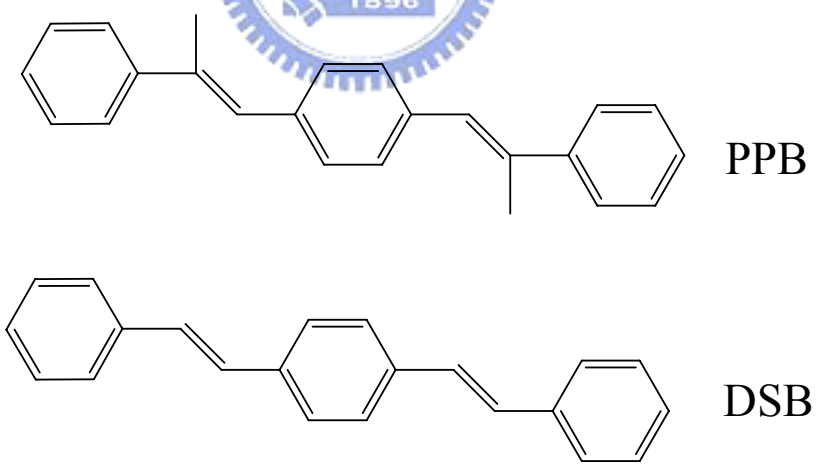

Scheme1: Chemical structures of PPB and DSB

In order to gain better understanding for this unusual phenomenon, we have

[7] (a)Fu, H. B.; Yao, J. N. *J. Am. Chem. Soc.* **2001**, *123*, 1434. (b)Fu, H. B.; Loo, B. H.; Xiao, D.; Xie, R.; Ji, X.; Yao, J.; Zhang, B.; Zhang, L.*Angew. Chem. Int. Ed.* **2002**, *41*, 962. (c) Xiao, D.; Xi, L.; Yang, W.; Fu, H.; Shuai, Z.; Fang, Y.; Yao. J. *J. Am. Chem. Soc.* **2003**, *125*, 6740.
[8] An, B.-K.; Kwon, S.-K.; Jung, S.-D.; Park, S.-Y. *J. Am. Chem. Soc.* **2002**, *124*, 14410.

investigated the excited-state relaxation dynamics and undertaken structural identification for free molecule and nanoparticles using the techniques of Field Emission Scanning Electron Microscopy (SEM), femtosecond (fs) and picosecond (ps) time-resolved fluorescence spectroscopy, and powder and single-crystal X-ray diffractions (XRD). The nanostructure samples are prepared according to the reprecipitation method in water/THF solutions. As water volume fraction exceeds 65 %, the nanoparticle of PPB starts to appear in solution. For PPB nanoparticles, two emissive states were observed in fluorescence transients and confirmed by the powder XRD measurements with two different packing structures. Fs fluorescence dynamics measurements have shown the significance of molecular geometry that affected the relaxation dynamics in the excited state of free molecule: efficient isomerization deactivation in PPB was observed, and the twisted nature of the geometry accelerated the rotational non-radiative process. In combination with the versatile results obtained in this study, we conclude that the enhanced emissions in PPB nanoparticles reflects the geometrical change from the twisted conformation to the nearly planar one in order to form the herringbone-type aggregation of nanoparticles, which is shown in the single crystal structure of PPB.

3.2 Experimental Section

Materials. The synthesis of PPB molecules was described elsewhere.[9] PPB was synthesized by Heck coupling.[10] A mixture of α-methylstyrene (2.5 g, 25.4 mmol), 1, 4-dibromobenzene (2.0 g, 8.4 mmol), palladium (II) acetate (0.037 g, 0.16 mmol), tris-(*ortho*-tolylphosphine) (0.102 g, 0.33 mmol) and triethylamine (4.92 g, 48.78 mmol) was prepared in thick-walled screw capped glass tube. The tube was capped under argon and heated overnight at 120°C. After cooling, the mixture was extracted with ethyl acetate, and the organic layer was washed with saturated NaCl and water by turns. It was dried with $MgSO_4$ and filtered, and then crude solid was recrystallized from hexane to get fine transparent crystals (yield: 65%).

Formation of Nanoparticles. The PPB nanoparticles were prepared by a simple reprecipitation method. Water and THF was used as a non-solvent and solvent, respectively. Volume fractions of water were controlled from 0 through 80%, with vigorous stirring at room temperature. In all solutions, the concentration of the chromophore (2.9×10^{-5} M) was constant after adding distilled water. After 65% volume fraction of water addition, PPB in mixture solution started to aggregate into nanosize particles. Nanoparticles' suspensions were homogenous and stable even after four months. Colloid sample for powder and SEM studies were prepared by the following procedures: the sample was first dispersed in THF and then dropped on a glass substrate (for powder XRD) or a carbon tape (for SEM) until it dried. The

[9] Bhongale, C. J.; Chang, C.-W.; Lee, C.-S. and Diau, E. W.-G. *J. Phys. Chem. B* **2005**, *109*, 13472-13478.

[10] Dieck, H. A.; Heck, R. F. *J. Am. Chem. Soc.* **1974**, *96*, 1133.

drop-dry process was preformed several times in order to deposit enough colloid samples.

X-ray Crystallography. (a) Powder XRD Collections. X-ray powder diffraction data were collected using a Bruker D8 diffractometer with Bragg-Brentano geometry (40 kV, 40 mA), Cu Kα radiation (λ= 1.5406 Å), and a 40 mm Göbel mirror. For a bulk sample, the powder pattern was scanned over the angular range 5-60° (2θ) with a step length of 0.1° and a counting time of 4 s per step. For a colloid sample (bulk and 65-80% solutions), the pattern was scanned over the angular range 5~16° (2θ), with a step length of 0.02° (2θ) and a counting time of 10 s per step. The measurements were carried out at room temperature. **(b) Single-crystal XRD Collections.** Single crystal suitable for the X-ray diffraction study was prepared from the slow evaporation of PPB in THF solution. A crystal with an average cubic shape (0.1×0.1×0.1 mm) is selected under an optical microscope, glued on glass fibers, and then mounted on an Enraf-Nonius CAD4 diffractometer using Mo Kα radiation (λ = 0.71073 Å) and ω-2θ scan mode. The SEARCH procedures were carried out for orientation matrix determination and peak indexing on the basis of 25 observed reflections. An orthorhombic cell was initially found a = 6.30(2) Å, b = 7.56(2) Å, c = 36.7(7) Å, V = 1750(3) $Å^3$. A datum collection of reflections was performed in 2θ ranges from 2 to 55°. No significant intensity variation was observed during the acquisition for the three standard reflections chosen for each recording. The crystal revealed a orthorhombic unit cell (a = 6.3218(13)Å, b = 7.555(2)Å, c = 36.774(7)Å, V =1756.4(6)$Å^3$). All carbon atoms were refined with isotropic displacement parameters and the H atoms are added manually, and their positions and thermal parameters are

fixed.

Computational Methods.

The structures of the isolated PPB and DSB molecules were determined by the density functional theory (DFT) methods implemented in the Gaussian 03 software package. The geometries of the molecules in the ground state were optimized at the B3LYP/6-31G(d) level of theory with the vibrational frequencies calculated at the same level being all positive numbers.

3.3 Results and discussion

3.3.1 Formation of PPB nanoparticles

A series of PPB nanoparticles with various percentage of water volume fractions viz. 0, 50, 55, 60, 65, 70, 75 and 80%, were prepared by the simple reprecipitation method using water as a poor solvent in THF. The evidence of the nanoparticle suspension was observed with the appearance of turbidity in the mixed solution when the volume fractions of water exceeded 65%. The color of solutions becomes deepened as the volume fractions of water increase from 65 to 70%. In addition, the size of the nanoparticles increased as a function of the volume fraction of water addition. Figure 3.1 shows the SEM photographs of PPB nanoparticles with different average particle sizes at various water volume fractions of solutions: (A) 50 nm at 65%; (B) 150nm at 70%; (C) 300 nm at 75%; (D) ~μm at 80%. It is observed that the free molecules in the solution starting to aggregate at 65% volume fractions of water addition.

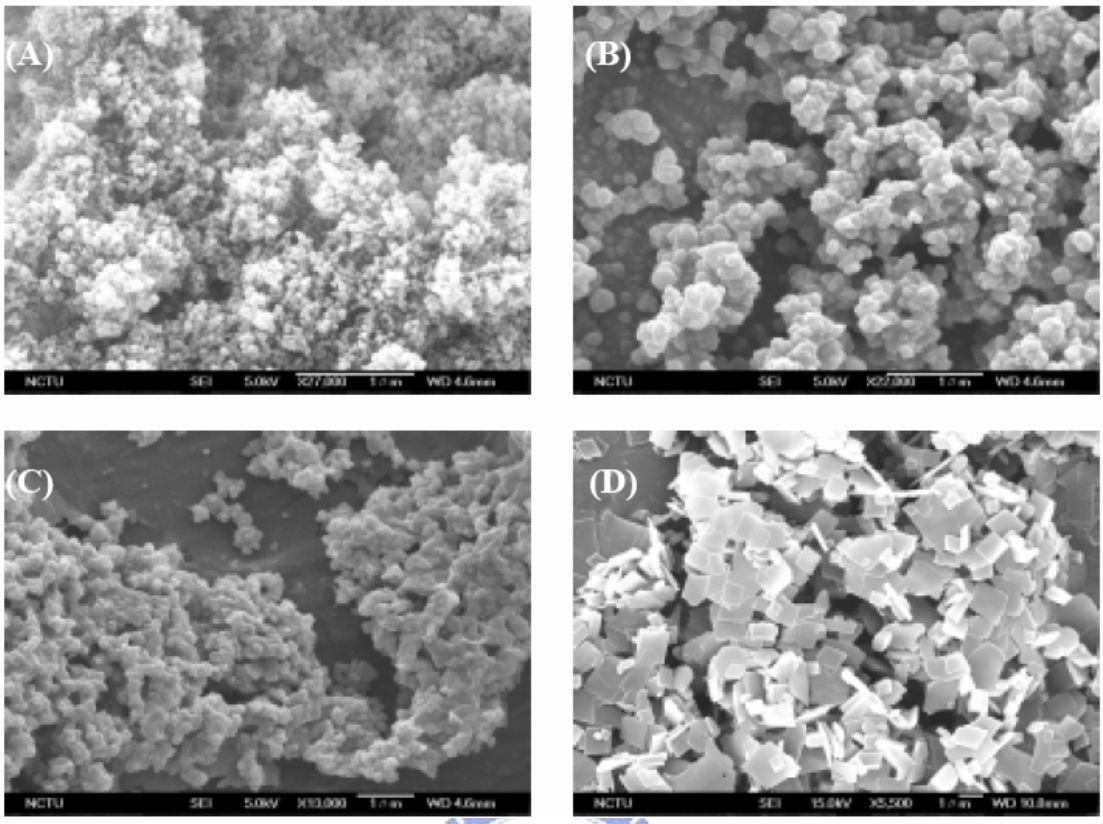

Figure 3.1: SEM images of PPB nanocrystals showing the sizes in average diameters of (A) 50, (B) 150, (C) 300 nm and (D) ~ μ m obtained from nanoparticle's suspension containing 65, 70, 75 and 80% volume fractions of water in THF, respectively.

In Figure 3.1, we found that the free molecule in the solution starting to aggregate at 65% volume fractions of water addition. In the preparation SEM samples, we need to dry the solvent on carbon tape, and aggregate might be formed. If the particle we observed is the aggregate formed during the evaporation, we should observe nanoparticles even in 0% water/THF solution, and the particle in all solution should the same. Therefore, we believed that the SEM image is not due to the aggregate formation during sample preparation. Initially, spherical shape particles were formed as the good solvent (THF) was replaced by the poor solvent (water). Therefore, the observing spherical shape of the nanoparticles is probably due to the minimization of interfacial energies between PPB and water molecules.[1] As the percentage of water addition became higher than 65%, the molecules aggregate to larger structures with

some germs of crystallization and the size of PPB nanoparticles increased dramatically. The size-dependent feature implies that the nanocrystallization of PPB proceeds as the water volume fraction of the solution increases, and it's because the water-insoluble PPB molecules aggregate together at higher water fractions. The size dependence in formation of PPB nanoparticles is similar to what has been reported recently in the cases of PDDP,[7a] DPP,[7b] and DAP.[7c] However, when the volume fractions of water addition increase up to 80%, the extraordinarily large particle size (~μm) is found, and the shape of the particle becomes rectangular (Figure 3.1D). The formation of rectangular nanoparticles in 80% solution is probably due to a competing process between the anisotropic growth and the spherical aggregation, which is similar to the case of recent study in evolving the one-dimensional nanostructures of *p*-BSP in water/THF mixtures.[1] In the present study, the size-dependent optical properties of the PPB nanoparticles are different from those of previous studies, which will be discussed in the following paragraphs.

3.3.2 Steady-state absorption/emission spectra

The UV/visible absorption spectra and the corresponding emission spectra at various volume fractions of water addition are shown in Figure 3.2A and 3.2 B, respectively. For the solutions of 0-65% water volume fractions, the UV/vis spectra (Figure 3.2A) feature a strong absorption band with maximum peak at 314 nm. As the water volume fractions increase to more than 70%, we observed the dramatic decrease in absorbance at 314 nm accompanying with the build up of new absorption band at 273 nm. The additional absorption band at 273 nm becomes more pronounced at 80%

solution. The blue-shifted nature in UV/Vis absorption spectra of the PPB nanoparticles is similar to what has been observed in the systems of DPST[8] and DSB.[11,12]

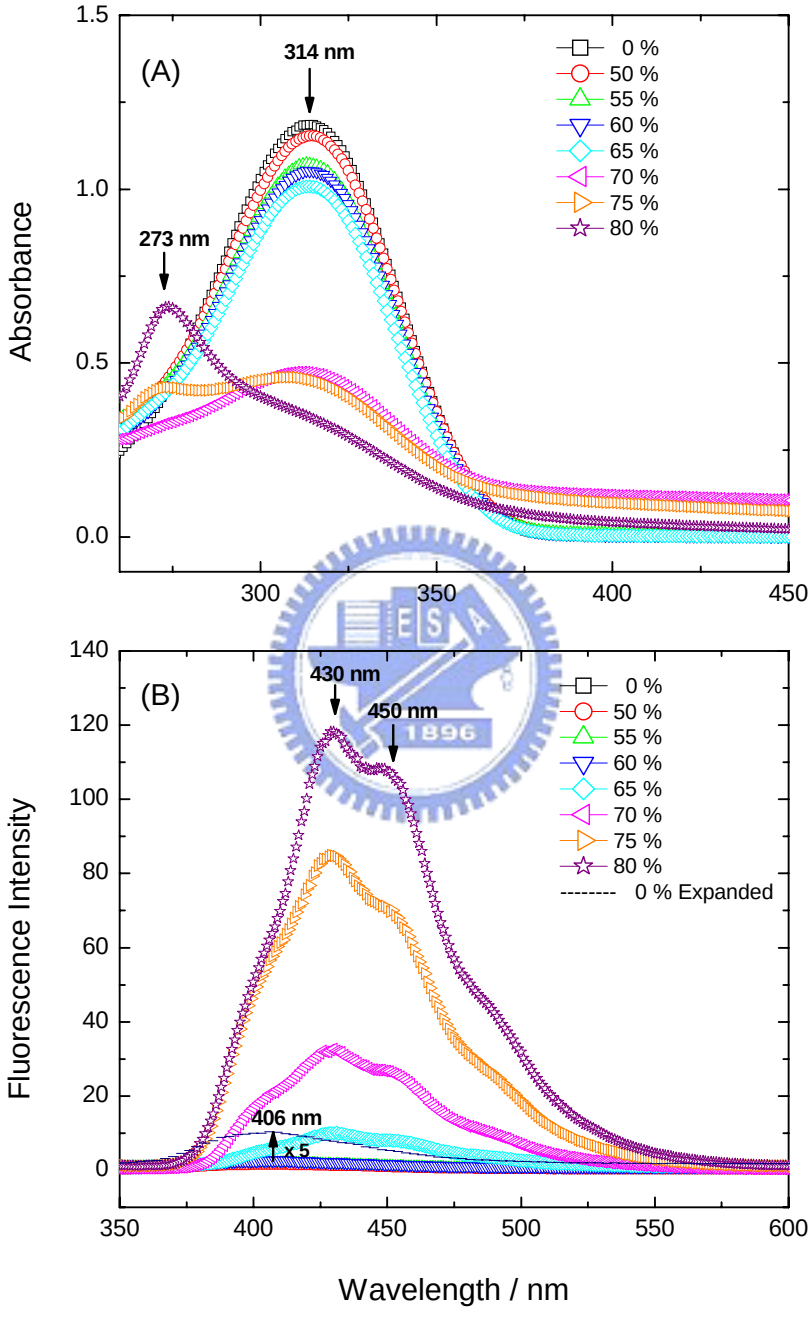

Figure 3.2: (A) UV-Visible absorption spectra changes of PPB depend on the water fractions in THF. (B) PL spectra changes of PPB depend on the water fractions in THF. The excitation wavelength was fixed at 310 nm.

[11] Oelkrug, D.; Tompert, A.; Gierschner, J.; Egelhaaf, H.-J.; Hanack, M.; Hohloch, M.; Steinhuber, E. *J. Phys. Chem. B* **1998**, *102*, 1902.
[12] Egelhaaf, H. J.; Gierschner, J.; Oelkrug, D. *Synthetic Metals* **1996**, *83*, 221.

The emission of PPB at 0–60% water volume fractions were hardly observed, which indicated the non-fluorescent nature of the free PPB molecule in solutions. In Figure 3.2B, the emission spectrum at 0% solution features a structureless broad emission band with the maximum peak at 406 nm. All the emission spectra with water volume fractions between 0–60 % are very similar in shape and intensity. As the water volume fraction becomes higher than 65 %, there are two new spectral features. First, the emission spectra at 65-80% solutions are distinctly shifted to a long wavelength region (peak maximum ~430 nm) with an apparent vibrational structure. Second, although the observed red-shifted emission spectra are all similar in shape, a substantial enhancement in intensity is found, and we found that the emission intensity increases with the particle size. (Figure 3.2B). Since the observed emission intensity systematically increases as a function of volume fractions of water addition, it reveals that formation of the PPB nanoparticles results in the enhancement of the emissions; the larger the particle size, the higher the emission intensity. This result is different from that of DPST[8] and DSB[11,12], in which the formation of nanoparticles accompany a substantial decrease in emission intensity.

The observed fluorescence enhancement in PPB nanoparticles is similar to that of CN-MBE nanoparticles.[8] In the literatures,[1,8] both intra- and intermolecular effects can be used to explain the observed fluorescence enhancement. Generally speaking, intramolecular effect assumes that the free molecules in solution undergo efficient nonradiative process via twisting motion, and the planar ones form in the solid state will suppress this channel. Intermolecular effect is arisen from intermolecular interactions when molecular aggregations become significant. This effect is strongly

dependent on the geometry of the packing structure. As described in the molecular exciton model,[13] two types of aggregations are involved: H-aggregates tend to accelerate the nonradiative relaxation process due to strong π-stacking interactions in the parallel aligned structures; J-aggregates, on the other hand, inhibit the nonradiative process for the molecules arranged in the head-to-tail direction. In the case of CN-MBE, the enhanced emission was attributed to both effects of intramolecular planarization and J-type aggregate formation in the nanoparticles, because a red shift in the UV absorption spectra was observed.[8] In our case, the UV spectra of PPB nanoparticles show a distinct blue shift (Figure 3.2A), which is usually an indication of the formation H-type aggregates. However, in figure 3.2B, the observation of the enhanced fluorescence cannot be explained by a usual H-type aggregation. More experimental evidence will be given in the following sections in order to understand the mechanism for the fluorescence enhancement of the PPB nanoparticles.

3.3.3 Picosecond relaxation dynamics of PPB nanoparticles

Time-dependent measurements of PPB in various water/THF solution mixtures were performed by TCSPC technique with excitation wavelength at 310 nm (λ_{ex}=310 nm), and probing at 420 nm (λ_{fl} = 420 nm). The transients are shown in Figure 3.3. The fluorescence decay in 0–60% volume fractions of water are all characterized exclusively by a sharp spike due to the limit of the time resolution of instrument response (~50 ps). However, the transient at 65% solution contains two major parts:

[13] Hans, K.; Försterling, H.-D. *Principles of physical chemistry: understanding molecules, molecular assemblies, supramolecular machines*; Wiley: New York, 2000

first part shows the fast-decay feature with the corresponding kinetics being instrument-limited; the second part shows a slow-decay character with the time coefficient in nanosecond time scale.

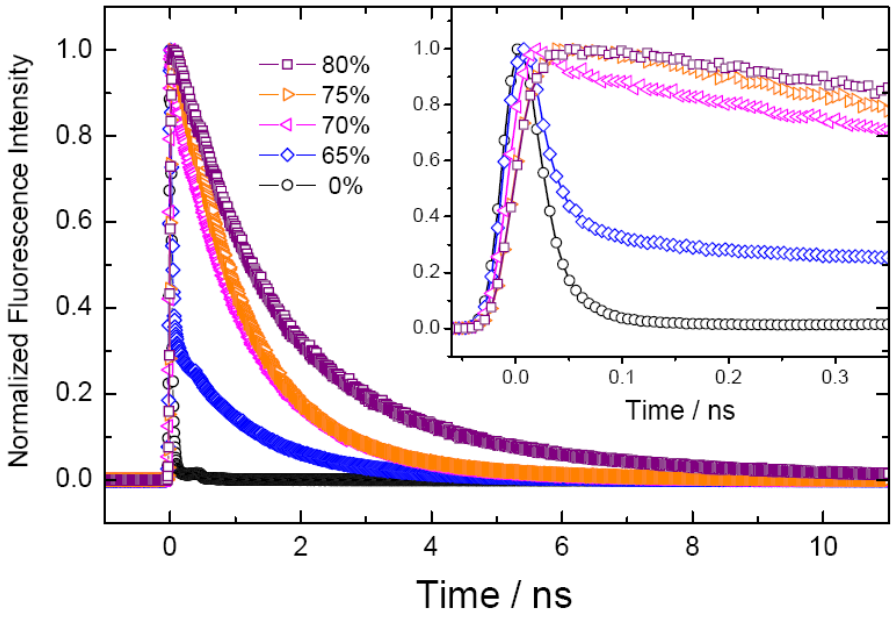

Figure 3.3: (A) Picosecond fluorescence transients of PPB shown in log scale are obtained from the excitation at λ_{ex} = 310 nm and the probe at λ_{fl} = 420 nm at various water/THF mixtures as indicated. (B) Picosecond fluorescence transients of PPB are shown in linear scale at 0, 65, 70, 75 and 80% solutions. The inset shows the corresponding transients in short time scale.

At 70% water volume fraction, the slow-decay part becomes the major component. When the water additions increase to 75% and 80%, the contribution of the fast-decay parts become negligible and the slow-decay parts become predominant in the transients. The above observations indicate that the formation of PPB nanoparticles leads to the formation of new components (the slow-decay part) in fluorescence transients with much longer excited-state lifetimes; the larger the nanoparticle size is, the more significant the slow-decay part becomes. This feature is consistent with the intensity enhancement in steady-state fluorescence spectra (Figure 3.2B). Since the fast-decay part arise from the contribution of free PPB molecules (studied by using

the femtosecond technique will be discussed below), we only focus on discussing the kinetic data of the PPB nanoparticles obtained from the 65–80% solutions. Figure 3.4A, B, and C show three typical transients of the 75% solution with λ_{ex} = 310 nm and λ_{fl} = 390, 450 and 510 nm, respectively

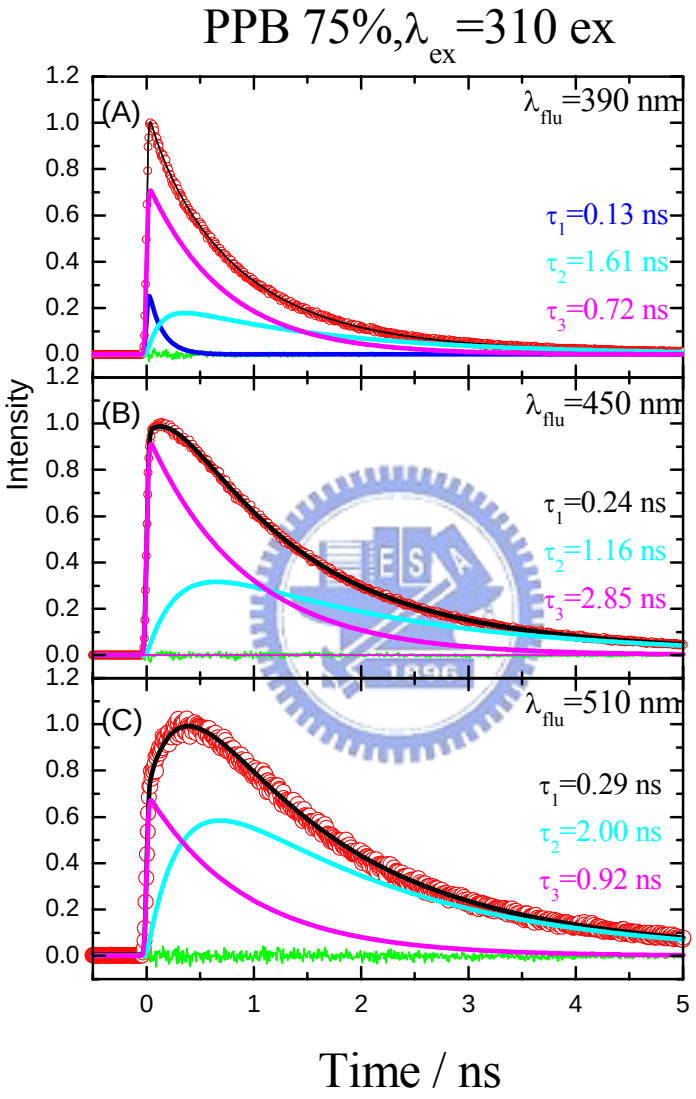

Figure 3.4: Picosecond fluorescence transients of PPB at 75% solution with λ_{ex} = 310 nm and λ_{fl}/nm = (A) 390, (B) 450 and (C) 510. The data are fitted according to the dual-emissive model (Scheme 2). The solid black curves are theoretical fits with residues shown as the green traces. The τ_1, τ_2 and τ_3 correspond to the A and B, and A′ in Scheme 2, respectively.

The transients show complex kinetic features, which cannot be described by a single exponential decay function. Since the transient at λ_{fl} = 510 nm clearly features

a rising character, a consecutive kinetic model, $A \xrightarrow{\tau_1} B \xrightarrow{\tau_2} C$, should be utilized for the curve-fitting procedure. In this Model, A represents the initial Franck-Condon (FC) state upon excitation, B stands for the excited state of the PPB nanoparticles (bright state), and *C* represents the ground state of the nanoparticles (dark state). The result indicates that the FC state decays with a time coefficient, τ_1, while the bright state builds up in τ_1 and then decays to the dark state in τ_2. This kinetic model is consistent with the dual-state model utilized in fitting the kinetic data of the DSB aggregates, in which A represents the intrinsic excitonic state and B for a low-energy defect state.[14]

Even though the consecutive Model was able to describe the rise and decay feature of the transients, the fitting quality of the decay part was not satisfying. In order to solve this problem, another component (*A′*) was added in the consecutive kinetic model (as shown in scheme2), while *B′* was produced parallel with *B*. In this case, *A′* represents another bright state of the PPB nanoparticles, and the structure might be different from component A. Based on this Model, all transients of 65-85% solutions can be described well, and the fitted parameters are summarized in Table 1, and Figure 3.5 shows the fitting time coefficient as a function of fluorescence.

For comparison, we also measured the time-resolved transient of the PPB crystal. We found that the transients of bulk single crystal of PPB involve no rising character, and can be well fitted by a single-exponential decay with minute offset. (Appendix B) According to the above kinetic analysis of the fluorescence transients, three dynamical features of the excited PPB nanoparticles emerge.

[14] Lim, S.-H.; Bjorklund, T. G.; Bardeen. C. J. *J. Phys. Chem. B* **2004**, *108*, 4289.

Table 1. Fitted time constants of PPB in various volume fractions of water/THF solutions at λ_{ex} = 310 nm.[a,b]

λ_{fl}	390 nm				420 nm				450 nm			
	65%	70%	75%	80%	65%	70%	75%	80%	65%	70%	75%	80%
τ_1/ns	0.31 (0.04)	0.05 (0.19)	0.13 (0.25)	0.09 (0.26)	0.26 (0.14)	0.30 (0.08)	0.22 (0.06)	0.23 (0.15)	0.26 (0.16)	0.39 (0)	0.29 (0)	0.23 (0.18)
τ_2/ns	1.00(0.02)	1.48 (0.08)	1.61 (0.17)	2.30 (0.19)	1.26 (0.10)	1.79 (0.16)	2.04 (0.17)	3.45 (0.23)	1.66 (0.19)	1.78 (0.35)	2.00 (0.31)	4.03 (0.35)
τ_3/ns		0.68 (0.19)	0.72 (0.58)	0.94 (0.55)		0.87 (0.60)	0.88 (0.77)	1.16 (0.63)		0.92 (0.65)	0.92 (0.69)	1.45 (0.47)
τ /ns[c]	0.02 (0.94)	0.01 (0.55)			0.02 (0.75)	0.03 (0.16)			0.02 (0.65)			
λ_{fl}	480 nm				510 nm				540 nm			
	65%	70%	75%	80%	65%	70%	75%	80%	65%	70%	75%	80%
τ_1/ns	0.35 (0.14)	0.41 (0)	0.32 (0)	0.31 (0.17)	0.39 (0.10)	0.41 (0)	0.32 (0)	0.36 (0.13)	0.40 (0.07)	0.45 (0)	0.32 (0)	0.42 (0)
τ_2/ns	1.78 (0.23)	1.73 (0.50)	1.89 (0.45)	4.28 (0.43)	1.86 (0.22)	1.69 (0.59)	1.87 (0.54)	4.43 (0.49)	1.92 (0.18)	1.68 (0.63)	1.86 (0.62)	5.04 (0.48)
τ_3/ns		0.91 (0.50)	0.89(0.55)	1.71 (0.40)		0.88 (0.41)	0.92 (0.46)	2.07 (0.38)		0.88 (0.37)	0.92 (0.38)	2.52 (0.52)
τ /ns[c]	0.02 (0.64)				0.02 (0.68)				0.02 (0.75)			

[a]The numbers in brackets are the relative amplitudes; the value was set to zero if the contribution of the component was too small to fit. [b]All parameters were obtained according to the kinetic model shown in *Scheme 2* except the transients of 65% solution via a simple consecutive model. [c]Time constants due to free PPB in solution are instrument-limited (<30 ps). The deconvolution of each transient was shown in appendixA.

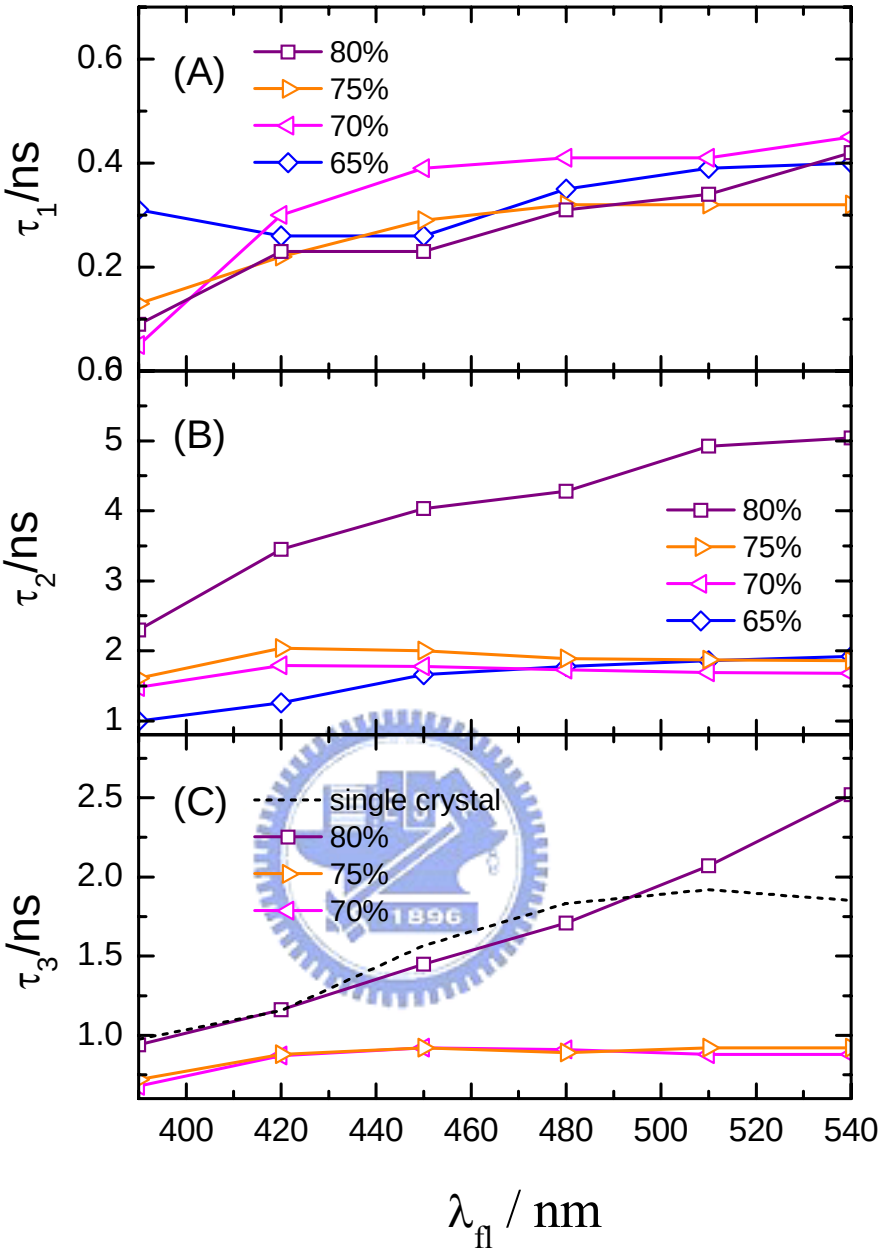

Figure 3.5: Three fitted temporal coefficients of PPB, (A) τ_1.(B) τ_2, and (C) τ_3. the corresponding fitted parameters are summarized in Table 1. The dashed curve shown in (c) represents the wavelength-dependent single-exponential-decay coefficient of the PPB single crystal.

SCHEME 2: A Dual-Emissive Model

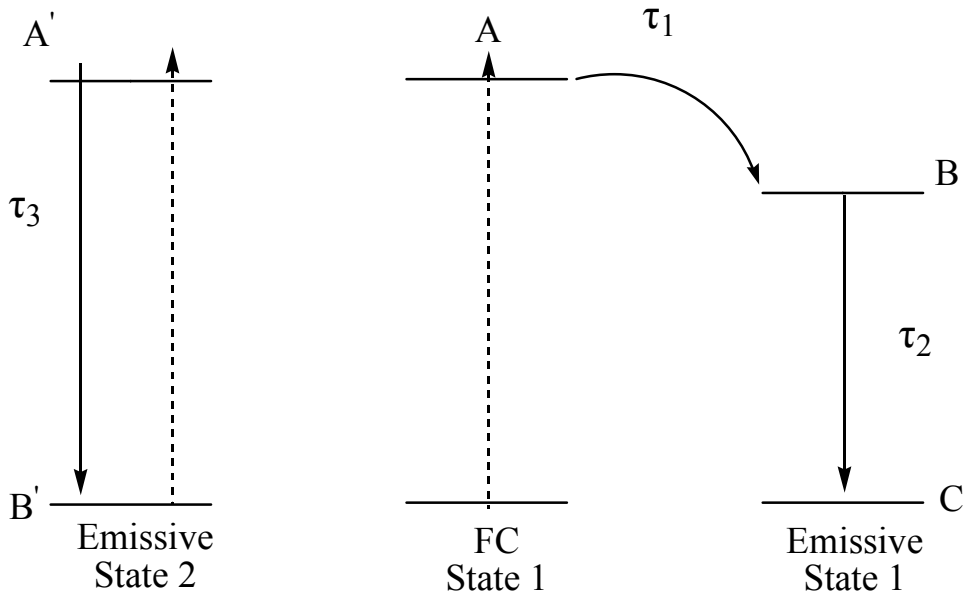

First, the observed time coefficients (Table 1 and Figure 3.5) are highly dependent on the probing wavelength. At longer wavelength, the fluorescence is emitted from the more relaxed state.[15] The systematic increasing in all time constants (τ_1–τ_3) as a function of λ_{fl} indicates that the energy-dependent nature of the relaxation in excited states of the nanoparticles.

Second, τ_2 and τ_3 are size-dependent, i.e., longer lifetimes are observed at larger nanoparticle size, and this relationship is more pronounced for τ_3. This size-dependent behavior on emission lifetimes was also reported for the systems of anthrance and DAP nanoparticles. Fluorescence quantum yield (Φ_F) can be obtained from the ratio of τ_f/τ_r, where τ_r is the time coefficient of the radiative process, and τ_f is the fluorescence lifetime. Assuming the radiative lifetime τ_r of free PPB and PPB nanopaticles is similar; the observed longer τ_f means the greater Φ_F. That explains the

[15] Lu, Y. C.; Chang, C. W.; Diau. E. W. G. *J. Chin. Chem. Soc* **2002**, *49*, 693.

increase in the emission intensity is the result of growth in nanoparticles. (Figure 3.2B).

Third, τ_3 for the 80% solution matches the decay coefficient of the single crystal with a lifetime in the range 1-2 ns, indicating a similarity between emissive state 2 in PPB aggregates (Scheme 2) and PPB bulk crystal. Therefore, the observing τ_3 was attributed to the fluorescence decay from the single crystal like structure in PPB aggregates. PPB aggregates in emissive state 1 were produced from the initial FC state with a rise time τ_1 and then decay with τ_2; this dual-state feature resembles that of DSB aggregates, in which the observed non-exponential fluorescence decays were modeled by two coupled excited states via an energy-transfer process from the excitonic state to the defect state, and it was similar to the procedure in our kinetic Model I mentioned previously.

To provide structural information for the two emissive states, the X-ray diffraction experiments based on the colloid samples of the 65-85% solutions were carried out.

3.3.4 Molecular structures of PPB in solid state and in solution

Powder XRD patterns of the colloid samples with different water additions (65-85%) are shown in Figure 3.6B. In the 2θ ranges of 6-15°, there are two diffractions at 2θ = 9.6° and 14.5° corresponding to [004] and [006] diffraction planes of the bulk materials. On the other hand, a new diffraction peak at 2θ = 7.3° (d = 12.2 Å) is clearly observed in XRD data of all 65-80% samples, and the diffraction intensity at 2θ = 7.3° shows no direct correlation for the samples of different water additions. The new diffraction peak suggests that a new type of three-dimensional

packing of the PPB molecules is formed when the colloid samples are prepared in the presence of H_2O.

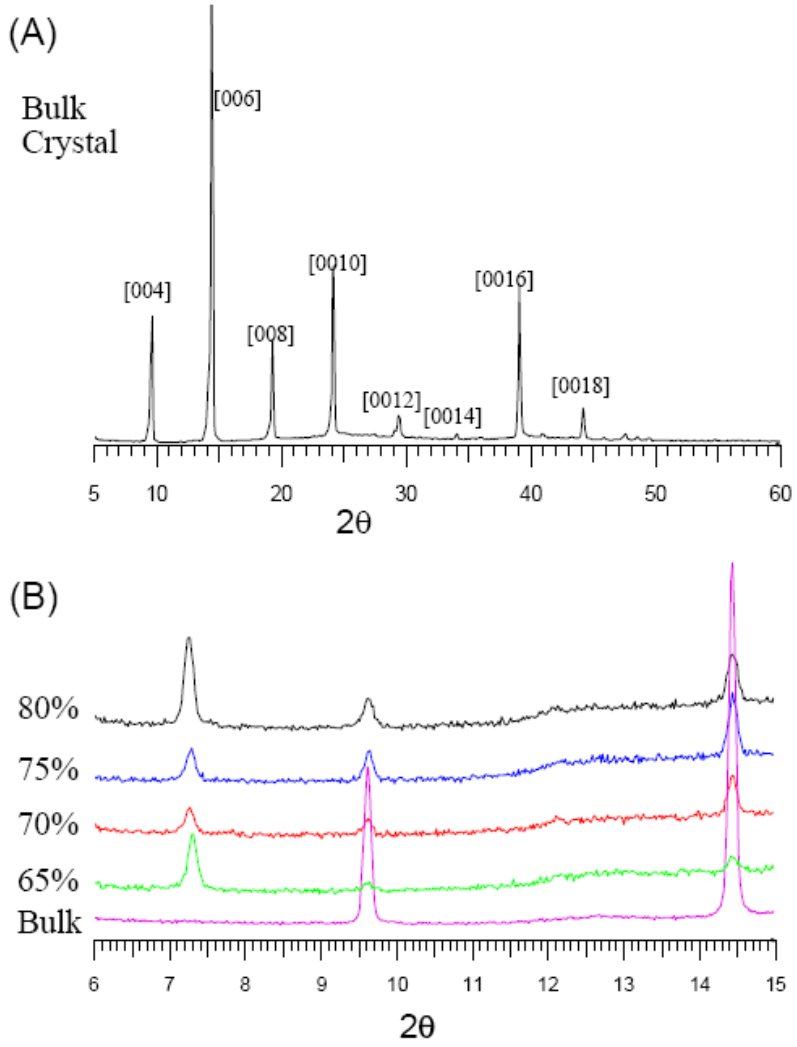

Figure 3.6: (A) Powder XRD pattern of the PPB bulk material. (B) Powder XRD patterns of the colloid PPB samples from various water/THF mixtures as indicated.

The presence of diffractions at both $2\theta = 7.3°$ and $2\theta = 9.6°/14.5°$ in water treated samples indicates that the water-induced PPB nanoparticles should contain two types of long range PPB packing structures. One is the same as the bulk material described below and the other is going to be uncovered. Because we do observe an induction period (τ_1 = 0.1–0.4 ns shown in Figure 3.4) for formation of the bright states, it is expected that water molecule may be involved in the unknown structure of the PPB

nanoparticles giving rise to the so-called "defect state" as proposed in the case of DSB aggregates.[14] The powder X-ray diffraction results have confirmed that two different packing structures are involved in the PPB nanoparticles. These result support our picosecond time-resolved experiments, in which we proposed two structures are exists in PPB nanoparticles.

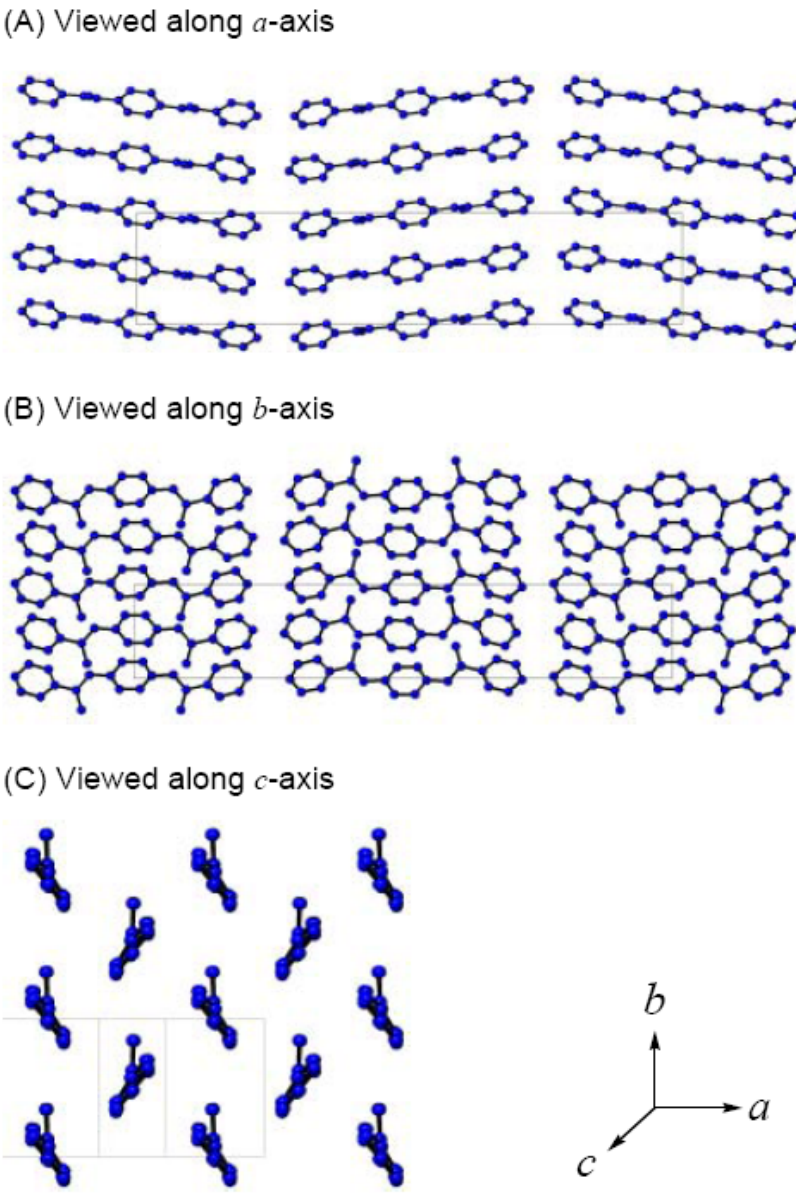

Figure 3.7: (A) Powder XRD pattern of the PPB bulk material. (B) Powder XRD patterns of the colloid PPB samples from various water/THF mixtures as indicated.

Single crystal suited for the X-ray diffraction study was prepared from the slow

evaporation of PPB in THF solution. Figure 3.7 shows the crystal structures of the plate-shaped PPB in three directions. There are four independent PPB molecules in a unit cell. The packing of PPB molecules alone *a*-axis shows the herringbone type structure (Figure 3.7A). Such molecular packing feature is similar to that of the chemically related compound (DSB). For each PPB molecule, the ethylene groups are parallel to *a*-axis and twisted with respect to the benzene ring in an average torsion angle of 31°. The direction of the ethylene groups in PPB molecule is shown in Figure 3.7B. For each PPB molecule, there are three benzene rings connected by two ethylene groups. Each ethylene group connects to two benzene rings in *trans*-form. The central benzene ring is connected with two phenyl groups via the ethylene bond in para- positions. It is apparent that the ethylene groups on 1,4-sites of the central phenyl ring are pointing to the same side.

The intermolecular packing of PPB molecules is shown in Figure 3.7C for a single layer of PPB molecules on the *ab* plane. The structure has been rotated 7° alone the *a*-axis to make the PPB molecule nearly perpendicular to the plane. It is quite obvious that each ethylene groups are parallel to the *a*-axis and twisted with respect to the benzene ring. The 2D packing of PPB molecule on the *ab* plane is close to the edge-to-face interactions of a 2×2 pinwheel, similar to that of DSB.[16]

For free PPB molecule, the structure was estimated using theoretical method. The structure was optimized at B3LYP/6-31G(d) level of theory. The optimized structures of the isolated PPB and DSB molecules are shown in Figure 3.8A and B, respectively. The free DSB molecule has a perfect planar geometry with all atoms located in the

[16] Spano. F. C. *Synth. Met.* **2001**, *116*, 339.

same symmetry plane, but surprisingly the structure of the free PPB molecule is non-planar with one end benzene ring twisted out of the molecular plane by ~80°. Note that the molecular structure of the free PPB molecule (Figure 3.8A) is entirely different from the structure in single crystal (see Figure 3.7B), where the three benzene rings in the latter are aligned parallel to a symmetry plane similar to the planar geometry of the free DSB molecule (Figure 3.8B).

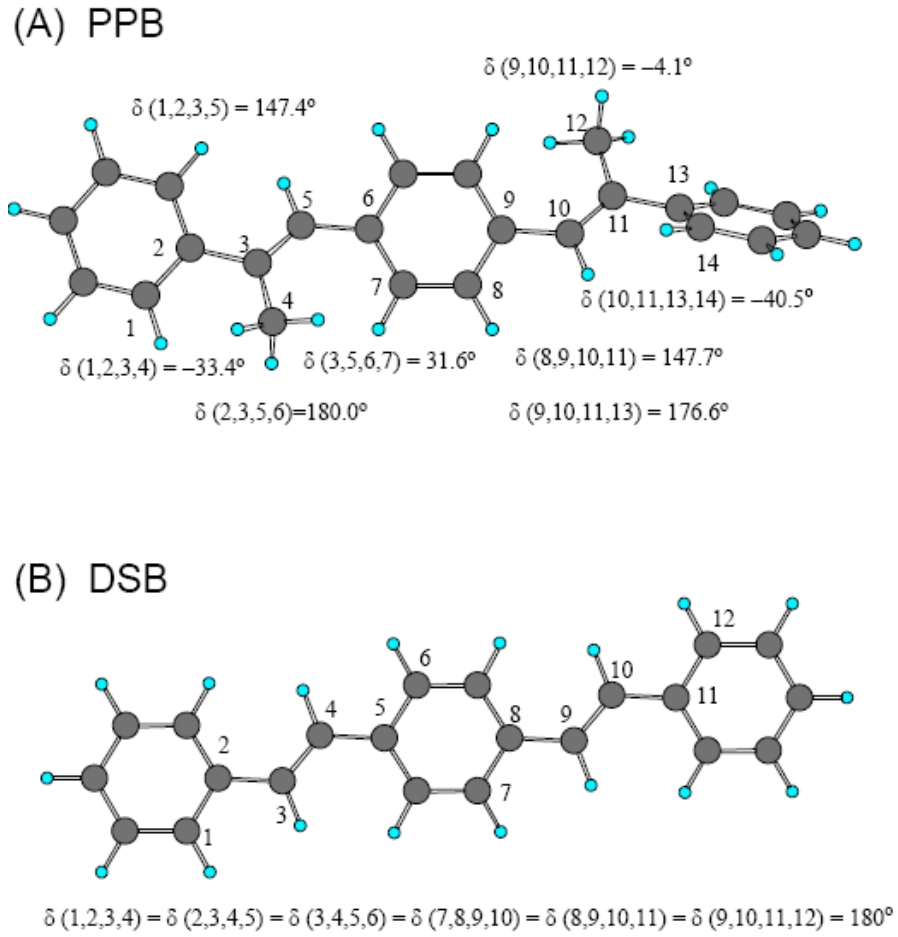

Figure 3.8: The ground state structures of (A) PPB and (B) DSB optimized at the B3LYP/6-31G(d) level of theory. The relevant torsional angles are indicated.

The correlation of the emission intensities on molecular structures of PPB between the solution and the solid phases has been found: the twisted conformation of the free PPB molecule is essentially non-fluorescent in dilute solution while the near planar geometry of the PPB unit cell in nanocrystals gives very strong emission in the solid

state. The conformational planarization of the PPB molecules when forming the nanoparticles seems to be the reason for the observed emission enhancement in the solutions of 65-80%. To further understand how the molecular planarity affecting the excited-state relaxation dynamics, we performed femtosecond fluorescence up-conversion measurements for both PPB and DSB molecules in dilute THF solution.

3.3.5 Femtosecond relaxation dynamics of free PPB and DSB molecules in THF

The structures of isolated PPB and DSB molecules are intrinsically different (Figure 3.8). The twisted geometry of PPB might due to the balance between strong hyper-conjugation of the methyl groups with the individual benzene rings and the long-range conjugation across all benzene rings. On the other word, PPB in dilute solution is nearly non-fluorescent, but free DSB molecules do give strong emissions.[11,12] Figure 3.9A and B show two typical fluorescence transients taken at λ_{ex} = 355 nm and λ_{fl} = 450 nm for PPB and DSB in THF, respectively. Apparently, the fast kinetics of PPB in 0% solution has now been unraveled. The transients were analyzed according to a proper kinetic model with convolution of instrument response function. For PPB, the transient are fitted with the combination of an independent exponential decay ($A' \xrightarrow{\tau_1} B'$) and a consecutive model ($A \xrightarrow{\tau_2} B \xrightarrow{\tau_3} C$). The decay time constants of τ_1, τ_2, and τ_3 are 1.3 ps, 9.2 ps and ~ns, respectively. For DSB, a consecutive model ($A \xrightarrow{\tau_1} B \xrightarrow{\tau_2} C$) is sufficient for an appropriate fit of the transient, where the two decay time constants are 13 ps and ~ns for τ_1 and τ_2, respectively. It reveals that the contribution of the ns component in the transient of

PPB is very minor while it becomes the major part of the transient in DSB.

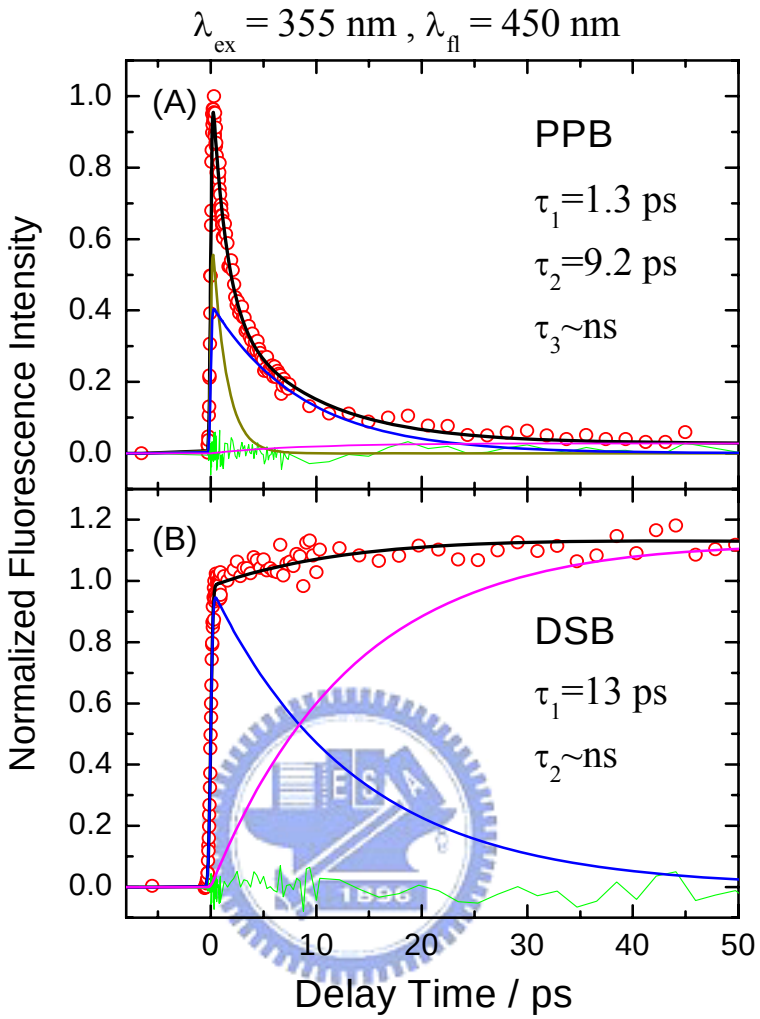

Figure 3.9: Femtosecond fluorescence transients of (A) PPB and (B) DSB in pure THF obtained from λ_{ex} = 355 nm and λ_{fl} = 450 nm. The transient of PPB was fitted according to a combined consecutive kinetic model, $A' \xrightarrow{\tau_1} B'$ and $A \xrightarrow{\tau_2} B \xrightarrow{\tau_3} C$, while that of DSB by a simple consecutive model, $A \xrightarrow{\tau_1} B \xrightarrow{\tau_2} C$. The solid black curves are theoretical fits with residues shown as green traces; the blue and magenta curves under each transient are the deconvoluted components corresponding to *A* and *B*, respectively; dark yellow curve shown under the transient of PPB represents *A'*.

This result is coincident with the steady state results, in which no observable emission for the former whereas strong emission was observed for the latter. On the other hand, the contribution of the ~1 ps component is significant in the transient of PPB, but it is negligible in the transient of DSB.

The fast ps component is unambiguously shown in the transient of PPB and therefore plays an important role in reducing the contribution of the ~ns component of fluorescence transient. Since the free PPB molecule has a twisted geometry while the free DSB molecule is completely planar (Figure 3.8), the existence of a correlation between the molecular structure and the observed relaxation dynamics is evident and will be discussed in the following.

According to the results obtained from the isolated *trans*-stilbene molecule, a planar molecule with two benzene rings connected by an ethylene group in a *trans* form, and the nonradiative process in the first singlet excited state (S_1) is governed by the isomerization of the ethylene twisting reaction coordinate with an energy barrier of only 3.4 kcal mol^{-1}.[17,18] Taking into consideration of the photoisomerization mechanism of *trans*-stilbene for the systems of present study, the observed ps relaxation in non-planar PPB is the result of crossing a small energy barrier along the C=C rotation channel on the S_1 surface. An efficient $S_1 \rightarrow S_0$ internal conversion follows at the perpendicularly twisted conformation, (so-called "phantom state" in the system of stilbene)[17,18] so that the ns component is hardly observed. For the planar DSB molecule, the ps nonradiative deactivation through the C=C twisting motion was not observed, probably due to a high energy barrier involved along the isomerization channel in S_1 state. Solvent-induced vibrational relaxation (VR) will also compete with the barrier-crossing deactivation process, and this leads to the ~10 ps component in both systems. Since the isomerization deactivation is much slower than the VR process in DSB, the electronically excited molecules would preferentially lose their

[17] Baskin, J. S.; Banares, L.; Zewail, A. H. *J. Phys. Chem.* **1996**, *100*, 11920, and references therein
[18] Felker, P. M.; Zewail, A. H. J. Phys. Chem. **1985**, 89, 5420

vibrational energy in the S_1 state, so that the electronic relaxation can only occur in the "cold" S_1 state which gives rise to the prominent ns component observed in DSB.

3.3.6 Femtosecond relaxation dynamic of PPB and DSB nanoparticles

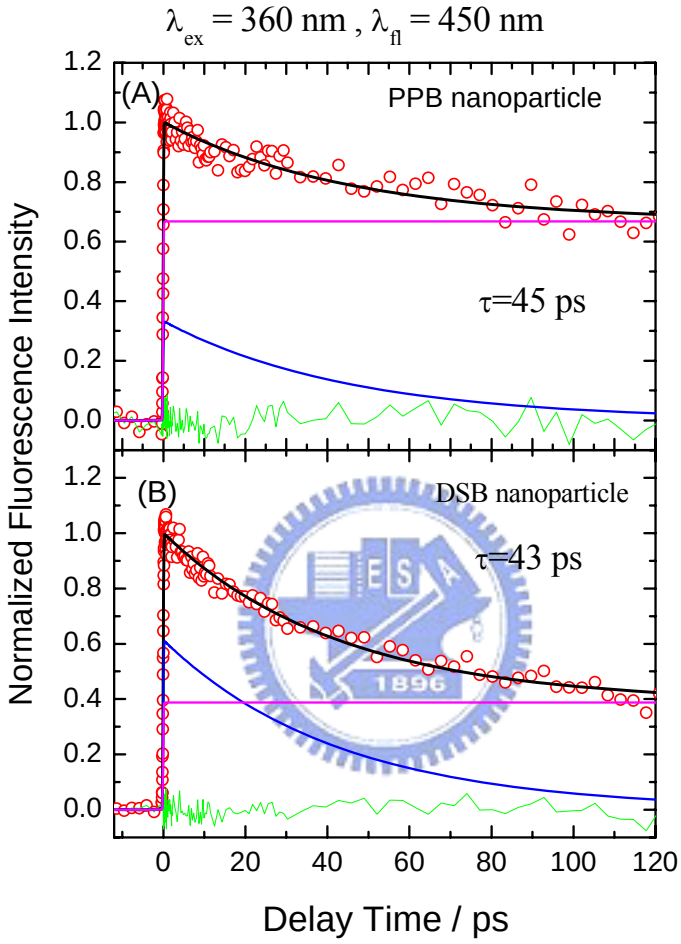

Figure 3.10: Femtosecond transients of (A) PPB and (B) DSB nanoparticles in 75% solution. The transient was obtained from λ_{ex}=360 nm and λ_{em}=450 nm. Both transient can be fitted by a bi-exponential function. The fast component (blue) decays ~45 ps, and the slow component (magenta) persists in 0~100 ps region.

Figure 3.10 , show two typical fluorescence transients taken at λ_{ex}=360 nm and λ_{em}=450 nm for PPB and DSB nanoparticles produced from the 75% solutions. Both transient can be fitted with a ~45 ps decay with an offset. In TCSPC experiment, because of the relatively worse temporal resolution , the ~45 ps is unresolved. Because the nuclear motions are restricted in nanoparticles, and the above-mentioned

rotational induced nonradiative process is inhibited. The observed 45 ps component in both systems might be due to the nonradiative deactivation process through intermolecular interactions involving π-stacking of the carbon backbones. In DSB nanoparticles, the relative amplitude of the 43 ps component is significant larger than in PPB nanoparticles, which states the stronger π-overlap interaction in solid state,[19,20] and this results in the much smaller quantum yield for DSB nanoparticles than for DSB in solution.[21]

3.4 Concluding Remarks

In the present study we reported the size-dependent optical properties of PPB nanoparticles prepared by reprecipitation in various volume fractions of the water/THF solutions and characterized by SEM, XRD, picosecond and femtosecond time-resolved laser spectroscopy methods. We observe strong emissions in PPB nanoparticles, but the emission of free PPB in dilute solution is hardly observed. In addition, fluorescence intensities of the nanoparticles systematically increased with the increasing of nanoparticle size. Femtosecond fluorescence measurements have shown that the nonradiative deactivation process through the ethylenic twisting isomerization channel was very efficient in PPB but inactivated in DSB. These dynamical behaviors were inferred due to the discrepancy of the structures between PPB and DSB in dilute solution, i.e., the twisted geometry of the PPB molecule should involve a small energy barrier for an efficient deactivation while the planar

[19] Wu, C. C.; DeLong M. C.; Vardeny, Z. V.; Ferraris J. P. *Synth. Met* .**2003**, 137, 939-941.
[20] Van Hutten, P. F.; Wildeman, J.; Meetsma, A.; Hadziioannou, G. *J. Am. Chem. Soc.* **1999**.121, 5910-5915.
[21] Oelkrug, D.; Tompert A.; Gierschner, J. Egelhaaf, H.-J.; Hanack, M.; Hohloch, M.; Steinhuber, E. *J. Phys. Chem. B* **1998**,102,1902-1907.

DSB molecule must involve a deactivation energy barrier that is too large to overcome in the excited state. This rationalizes the non-fluorescent nature of the twisted PPB molecule in dilute solution and establishes the concept of the molecular planarity giving strong fluorescent emissions in the PPB nanoparticles. The nearly planar geometrical nature of the PPB unit cell in the single crystal has been confirmed by our XRD studies. Moreover, powder XRD experiments demonstrated that there are two different packing structures involved in the PPB nanocrystals. One forms aggregates with the herringbone-type arrangement as observed in single crystal while the other is not yet to be determined. The dual-aggregate feature of the nanoparticles reflects the non-exponential kinetics in the picosecond time-resolved experiments for two emissive states being observed, one shows a single-exponential decay feature as observed in single crystal, and the other shows a rising feature assigned to be due to the unknown structure observed in the XRD data. In summary, we have found that PPB nanoparticles show weak emission in dilute solution but blue-shifted absorption and anomalously strong emissions in the aggregates. We provided experimental evidence for the enhanced emission of the nanoparticles being due to the combined effects of the conformational planarization, and the herringbone-type aggregate formed with an edge-to-face feature shown in the single crystal structure of PPB.